Surfaces and Interfaces 41 (2023) 103164

Contents lists available at ScienceDirect

Surfaces and Interfaces

journal homepage: www.sciencedirect.com/journal/surfaces-and-interfaces

Oxygen plasma induced solvent resistance of polystyrene particles enables the fabrication of ultra-thin free-standing crosslinked polymer films

Caitao Li [a,b], Tengfei Qiu [c], Guofu Zhou [a,b], Michael Giersig [a,d], Xin Wang [a,b], Eser Metin Akinoglu [b,a,*]

[a] International Academy of Optoelectronics at Zhaoqing, South China Normal University, Zhaoqing, 526238 Guangdong, China
[b] Guangdong Provincial Key Laboratory of Optical Information Materials and Technology & Institute of Electronic paper Displays, South China Academy of Advanced Optoelectronics, South China Normal University, Guangzhou 510006, China
[c] Nanomaterials Centre, School of Chemical Engineering and Australian Institute for Bioengineering and Nanotechnology, The University of Queensland, St Lucia, QLD, 4072, Australia
[d] Institute of Fundamental Technological Research, Polish Academy of Sciences, 02-106 Warsaw, Poland

ARTICLE INFO

Keywords:
Polystyrene particle
Oxygen plasma
Cross-linking
Solvent resistance

ABSTRACT

Plasma-treated polystyrene particles (PSP) are key building blocks in the fabrication of two- dimensional nanostructure arrays. Oxygen plasma etching can shrink PS particles and is a widespread tool in fundamental research and applications, but its effect has not been well understood. Here, we show that oxygen plasma induces an ultra-thin cross-linking layer on the surface of the PSPs, which increases their solvent resistance. We found in X-ray photoelectron spectroscopy (XPS) fine structure and valence band probing that the polymer C—C bonds are breaking and recombining to form oxygenated functional groups. Our results explain, why oxygen plasma etched PS particles are more difficult to dissolve in nanofabrication procedures. Further, we used the ultra-thin cross-linked polymer layer to construct novel substrate-base microcavity arrays.

1. Introduction

Two-dimensional nanostructure arrays have attracted much attention as they can be widely applied in photonic electronics, data storage, catalysis, sensors, and so on [1,2]. In the past few decades, colloidal particles, which are solid particles suspended in solvents, have played a significant role in the development of various nanostructure arrays such as hole, rod and dot arrays to realize diverse functions for plasmonics [3–5], magnetooptics [6], transparent conductor [7,8], advanced sensors [9,10], catalysis [11,12], and different areas of interface science [13,14] through the nanosphere lithography (NSL) technique, which became one of the most widely used nanofabrication tools in academic research due to its low cost, scalability, and versatility. Especially, polymeric, colloidal particles such as polystyrene (PS) particles have been popularly applied in NSL as these are easy to fabricate, modify and remove.

The modification of polymeric colloidal particles is the key for the controllable fabrication of a non-close-packed particle monolayer, which enables the fabrication of NSL-derived hole arrays and more complex nanostructures [15,16]. In fact, plasma treatment has been widely employed for material surface functionalization and modification to enhance their application performances, such as their improvement in the adsorption efficiency of adsorbents [17,18] and increased specific surface area of activated carbon [19,20]. But the most common modification is the use of oxygen plasma etching to reduce the size of the individual polymer particles without displacement.

At present, oxygen plasma treatment has been employed successfully for NSL [21,22]. But the interaction between the gas plasma and polymeric particles remains poorly understood. Previously it was shown that oxygen plasma exposed polystyrene surfaces can show a roughened surface because of polymer degradation, which was inducing or enhancing of surface cross-linking, i.e. dangling bond recombination after polymer backbone [23,24]. The gas plasma treatment process has noteworthy effects on the polymeric particles, which may affect the subsequence preparation of nanostructures and their final properties. Hence, understanding the changes of the polymer particle chemistry in response to the oxygen plasma will be significant to better control the quality of the achieved nanostructures and bring new opportunities in material design.

Here, we investigated the effect of oxygen plasma on PS particles and

* Corresponding author.
E-mail address: e.a@fu-berlin.de (E.M. Akinoglu).

https://doi.org/10.1016/j.surfin.2023.103164
Received 11 April 2023; Received in revised form 19 June 2023; Accepted 9 July 2023
Available online 11 July 2023

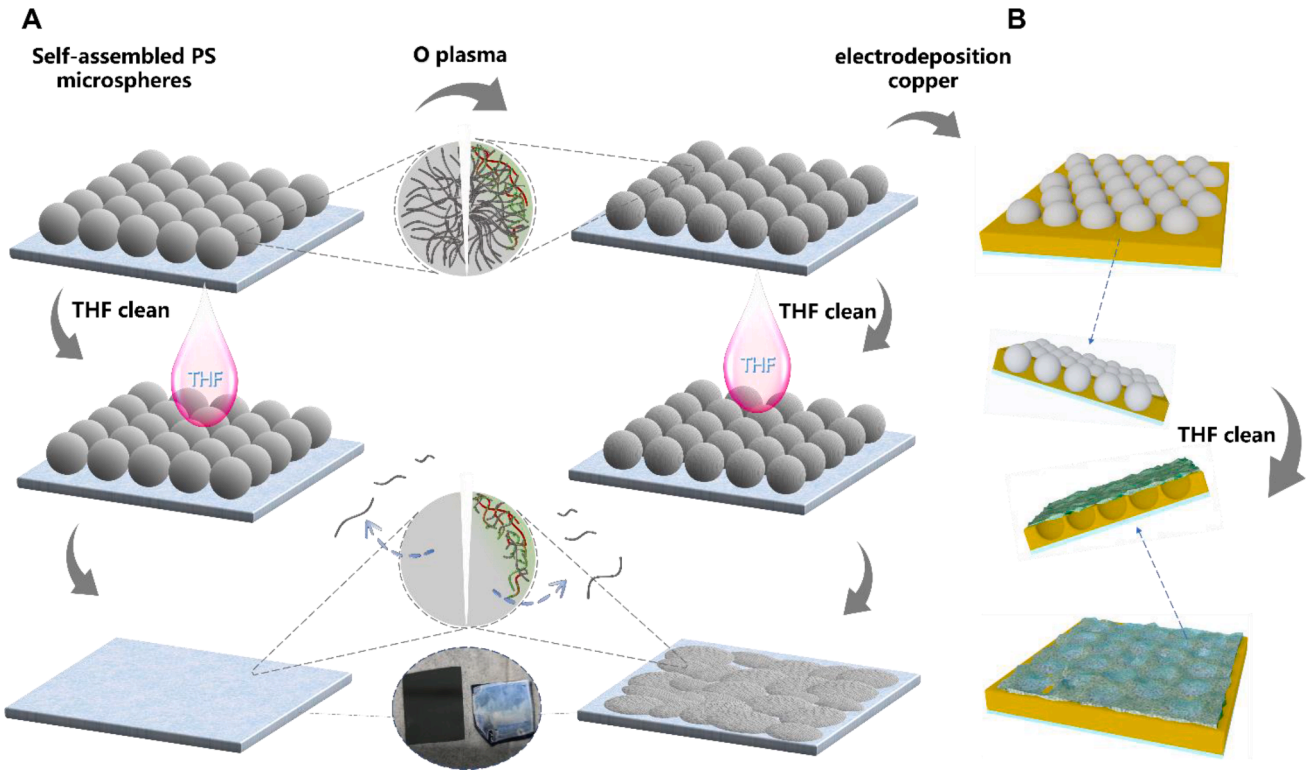

Fig. 1. Schematic illustration of (A) self-assembled PS particle monolayer on a flat substrate, which is exposed to an oxygen-containing plasma. A momentary plasma exposure as short as 10 s induces a chemical modification to the polymer chemistry in an ultra-thin layer at the particle top surface, which includes cross-linking and is shown as red bonds, before it can decrease the particle size. The short exposure of untreated PS monolayers to the THF solvent removes the whole particles formed by non-crosslinked PS. In the case of plasma-treated monolayers, the solvent cannot immediately dissolve the particles but must overcome the thin-crosslinked layer, which slows the PS dissolution and the cross-linked layer and deformed PS particles remain on the substrate after momentary solvent immersion and retraction. (B) Microcavities can be constructed by using plasma-treated PS monolayers as a template for electrodeposition of metal to fabricate an array of hemispherical metal cups. The removal of the PS particle bulk leaves the ultra-thin cross-linked polymer film anchored on top of these cups, which encloses cavities together with the metal cups.

show that the oxygen plasma treatment induces chemical transformation at their surface and forms an ultra-thin crosslinked layer, which cannot be dissolved by organic solvents. We demonstrate that this is the origin of the widely observed template lift-off resistance for oxygen plasma treated NSL templates. We further utilized the simple plasma-induced crosslinked polymer films to construct novel substrate-based microcavity arrays. These microcavities could enable to design and fabrication of novel microreactors, which, until now, are typically multichannel microscale or mesoscale reactors. Such reactors have high mass and heat transfer rate [25,26]. They also allow the testing of multiple reactions in sequence in a short time. Therefore, microreactors have shown great potential in the catalysis field. However, conventional phase-separated microreactors are restricted in liquid medium [27–29]. There is a lack of new technologies to realize a more sophisticated device structure available for broad working conditions. On the other hand, the complexity, controllability and high cost of current techniques still limits development in this area [30]. Our template-based microcavities have the potential to be used for photoelectrochemical reactions and exploit microlensing and light-concentrator effect. The cross-linked polymer films are permeable non-crosslinker polystyrene chains, and could therefore serve as permeable membranes to allow reactions in a two-compartment cell. These microcavities are easy to fabricate at low cost and the structure is highly controllable. The deployment of these microcavity arrays as microreactors will require to physical put catalysts particles into the cavities, which could be achieved by using inorganic catalyst encapsulated in PS microspheres in the future.

2. Experiment section

2.1. Reagents and materials

Reagent-grade copper sulfate, tetrahydrofuran (THF), sulfuric acid, absolute ethanol, toluene, acetone, isopropanol, sodium dodecyl sulfonate (SDS), and styrene were purchased from Aladdin Reagent Co., Ltd. In all experimental steps, 18 MW ultra-pure water was used. The polystyrene microsphere (500 nm diameter, 5 w% in H_2O) dispersion was purchased from Zhaoqing Chuangwei Nano Technology Co., Ltd.

2.2. PS particle monolayer fabrication

Glass slides (2 cm x 3 cm) were washed with acetone, ethanol, and ultra-pure water in an ultrasonic bath and dried with nitrogen. Electron beam evaporation (EBE) was used to deposit a 10 nm thick Ti adhesive layer followed by 100 nm Cu or Au deposition, which served as the substrate for PS particle monolayer deposition. As reported before, a solution containing PS stock solution, 1% styrene in ethanol, and 1% sulfuric acid in ethanol at a ratio of 30:30:1 was prepared to apply the PS particles to the surface of an ultra-pure water column situated in a glass petri dish and self-assemble the PS particles into a hexagonally arranged monolayer, which was evident to the bare eye by the opalescent colors. To ensure that we obtain a hexagonally close-packed monolayer, SDS was applied as a surfactant to the inner sides of the petri-dish to compress the PS particle monolayer. Finally, the substrates were immersed underneath the floating PS particle monolayer and lifted out of the water at an angle of 30° to deposit the PS particle monolayer on the substrates. The samples were left do dry naturally to evaporate all

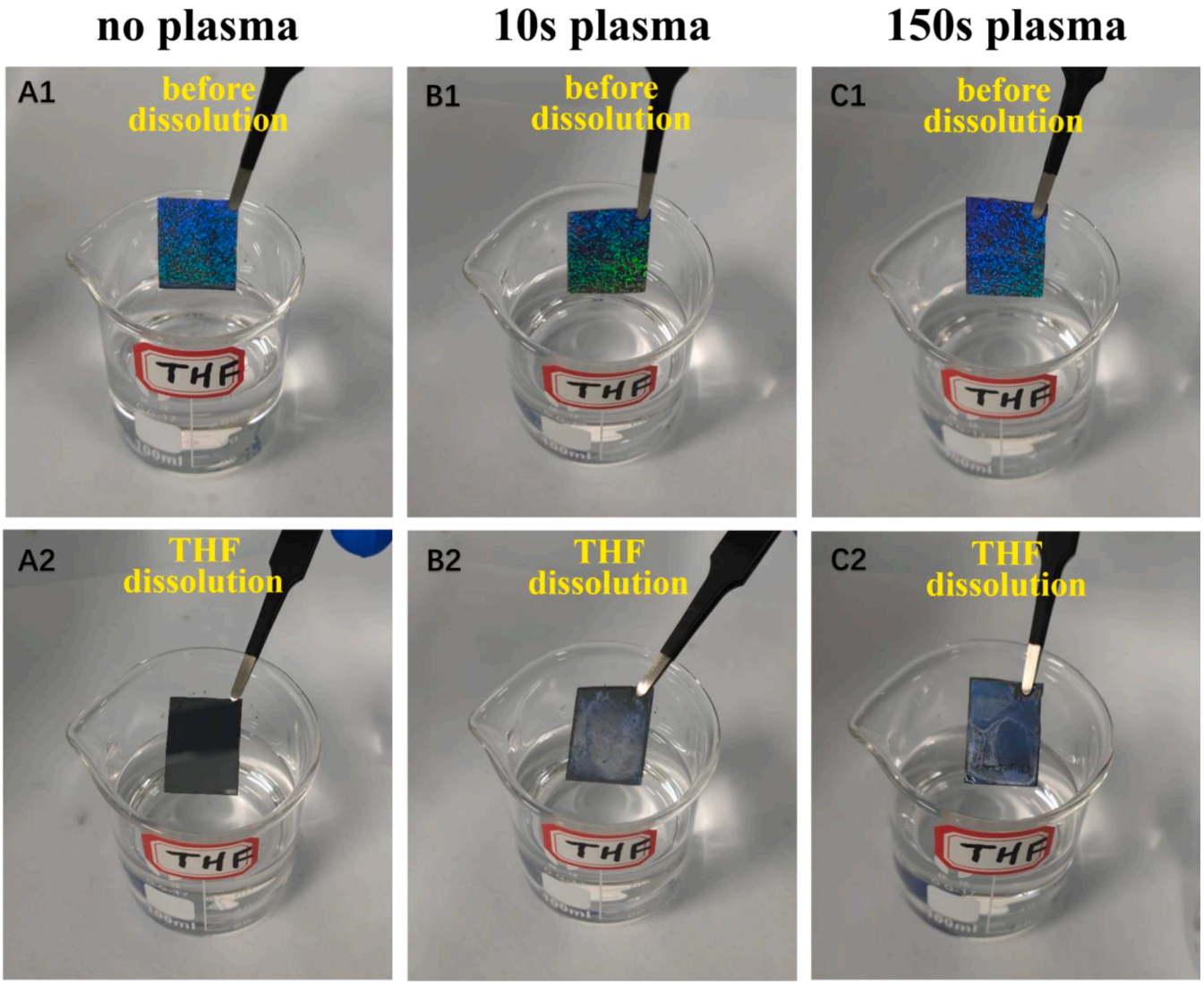

Fig. 2. Photographs of a (A) untreated, and (B) 10 s, and (C) 150 s oxygenated plasma treatment on 500 nm diameter PS particle monolayers on Si substrates. The plasma power was 30 W, under 20 Pa pressure and 10 sccm O_2 and 20 sccm Ar gas flow. The top row shows the that both the untreated and plasma treated samples show the characteristic opalescence because of their high crystallinity. These samples are then immersed into THF, which is an excellent solvent for polystyrene, for 10 s and retracted out of solution. The bottom row shows photographs of these samples after retraction from THF solution. While the untreated sample shows no remains of PS particles, the plasma treated samples show PS remains, which appear as white stains due to the loss of periodic order.

the water.

2.3. Plasma treatment

A radiofrequency (RF) plasma asher (CY-P2L-8100-Zhengzhou Chengyue Scientific Instrument Co., Ltd.) was used to treat the PS particles with an oxygen and argon gas mixture plasma. The etching power was set to 10 W, 30 W, and 50 W respectively and the gas flow rate for O_2 and Ar were 10 sccm and 20 sccm and the plasma pressure was controlled at 20 Pa. The cavity temperature was at room temperature before the start of the process and the etching time varied between 10 s and 150 s.

2.4. Copper electrodeposition

The electrolyte contains 2.25 g $CuSO_4$ dissolved in 1 L ultrapure water to a concentration of 9 mM. Concentrated sulfuric acid was added dropwise to adjust the pH to 1.35. Electrodeposition was performed using a three-electrode configuration in a 100 ml single cell compartment. The potential was controlled using a potentiostat (Chinstrument 600 E) to conduct chronopotentiometry. The PS particle monolayer coated copper film substrate served as the working electrode, while a platinum sheet counter electrode and an Ag/AgCl (3 M KCl) reference electrode were used respectively. Adjustment of the working potential to −0.427 V vs Ag/AgCl started the electrodeposition process and was continued for 10 min [31,32].

2.5. Polystyrene dissolution

The PS particles were cleaned by placing the samples into a beaker filled with tetrahydrofuran at room temperature to dissolve the PS particles for 24 h. In order to prevent the volatilization of tetrahydrofuran, the beaker was sealed with parafilm. Finally, the samples were removed and rinsed with ethanol, ultrapure water, and dried gently under a stream of nitrogen.

2.6. Sample characterization

The surface morphology and cross-sectional morphology of the samples were investigated using a Zeiss Sigma 500 scanning electron

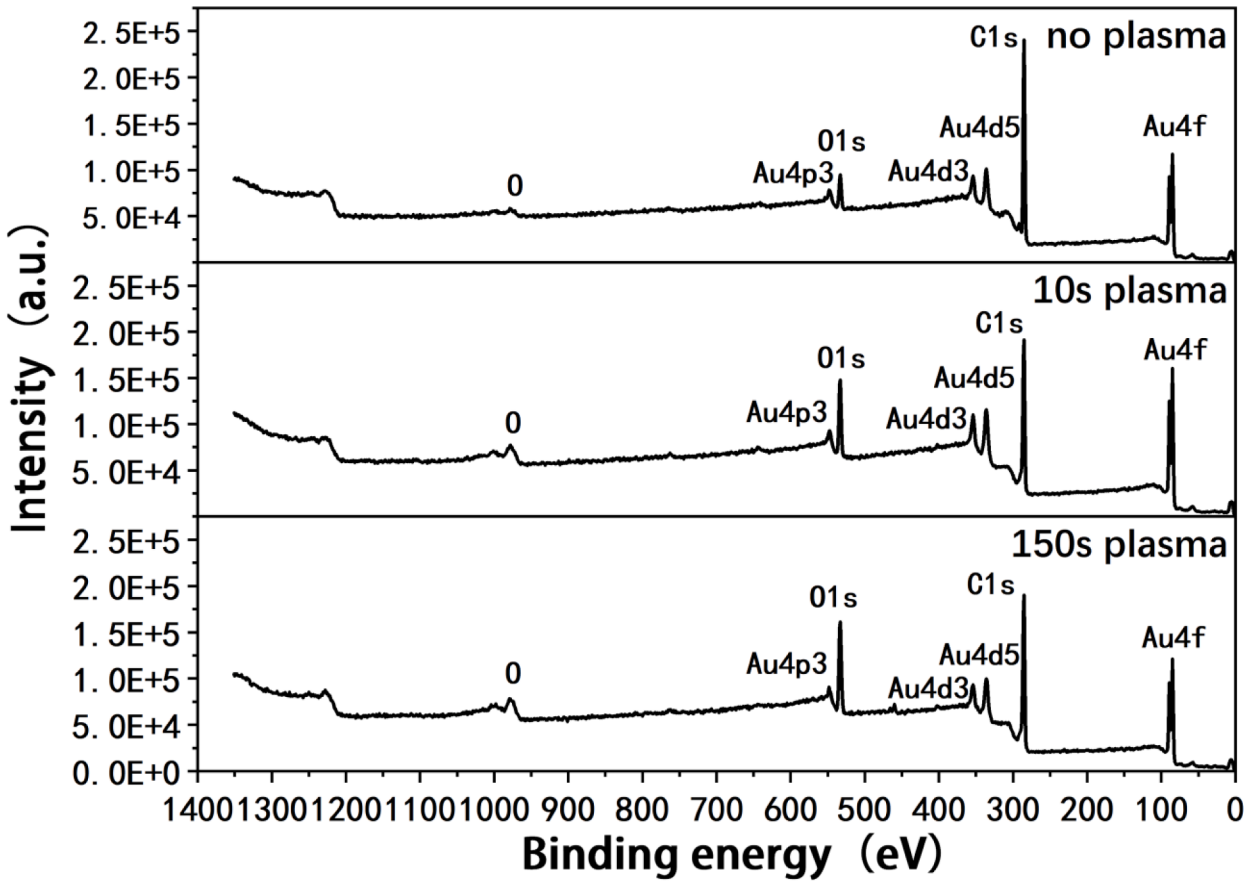

Fig. 3. XPS survey spectra of untreated and 10 s, 150 s oxygenated plasma treated PS particle monolayer on a 100 nm Au film. The plasma power was 30 W, under 20 Pa pressure and 10 sccm O_2 and 20 sccm Ar gas flow. The main peaks correspond to the Au 4f, C 1 s and O 1 s orbitals.

microscope (SEM). For each experiment, multiple areas on each sample were inspected, and these measurements were repeated on multiple samples to ensure the consistency of the results. Additionally, the topography of the samples was measured using a Bruker Dimension Icon atomic force microscope (AFM). Again, we performed these measurements on several areas of each sample, across multiple samples. The chemical composition of the PS particle surfaces was investigated using X-ray photoelectron spectroscopy (Thermo ESCALAB 250XI system) employing an AlKa X-ray source (1486.6 eV) to obtain chemical state information and collect valence band spectra of the pristine and plasma treated PS particles monolayers on a 100 nm Au film. For XPS, we measured three different areas for each sample to ensure a comprehensive representation of the chemical composition across the surface. The thickness of the membrane was measured at ten different locations and the mean thickness, as well as the standard deviation, was computed to provide an estimate of the variability of membrane thickness within the sample. All experiments were conducted at least three times to ensure the reliability of the observations.

3. Results and discussion

The experimental methodology and mechanism are depicted schematically in Fig. 1. We utilized a monolayer of PS microspheres as a template, which underwent oxygenated plasma etching. This treatment alters the polymer chemistry, such as inducing polymer crosslinking on the PS particle surface, thereby conferring resistance to organic solvents such as THF, toluene, and acetone. In contrast to untreated PS microspheres, which readily dissolve in these organic solvents, the plasma-treated PS particles display significant solvent resistance.

Residual PS remained on the sample surface, as shown in Fig. 1**A**. The elimination of these particles from the substrate surface required the application of ultrasonic treatment to aid in their detachment.

The cross-linked polymer surface can be exposed as a free-standing film (Fig. 1**B**) by first electrodepositing a metal like Cu through the plasma-treated PS microsphere array, which acts as a template to form metal bowls between the substrate surface and the PS particle monolayer.

The creation of the free-standing film only occurs as a later consequence of a slow, gradual process. Extended exposure to solvent over several hours led to the slow dissolution of the bulk of the PS particles. During this period, the PS chains migrated through the cross-linked surface film into the solvent. This progressive dissolution and migration eventually anchored the ultrathin cross-linked polymer films in place, stretching across the cavities between the metallic bowls. The result is a cross-linked polymer film that provides a noteworthy consequence of the plasma treatment's impact on the PS microspheres enabling the construction of microcavity arrays.

The visual consequences of the plasma treatment on the solvent resistance of the PS microsphere monolayer were distinctly examined. For this purpose, PS particles with a diameter of 500 nm were self-assembled onto polished silicon wafers, manifesting vivid, colorful characteristics due to opalescence. The colors were found to be largely unaffected by the oxygen plasma treatment using 30 W plasma power and exposure time from 10 s to 150 s (Fig. 2**A1-C1**), which indicate the PS particle monolayer remains intact; 10 W, 50 W plasma power treatment are shown in **Figure S1**.

However, upon vertically immersing these monolayers in THF for a period of 10 s, substantial disparities became evident between the samples. For instance, the monolayer formed by untreated PS microspheres was completely cleared by THF, leaving no visible traces of PS

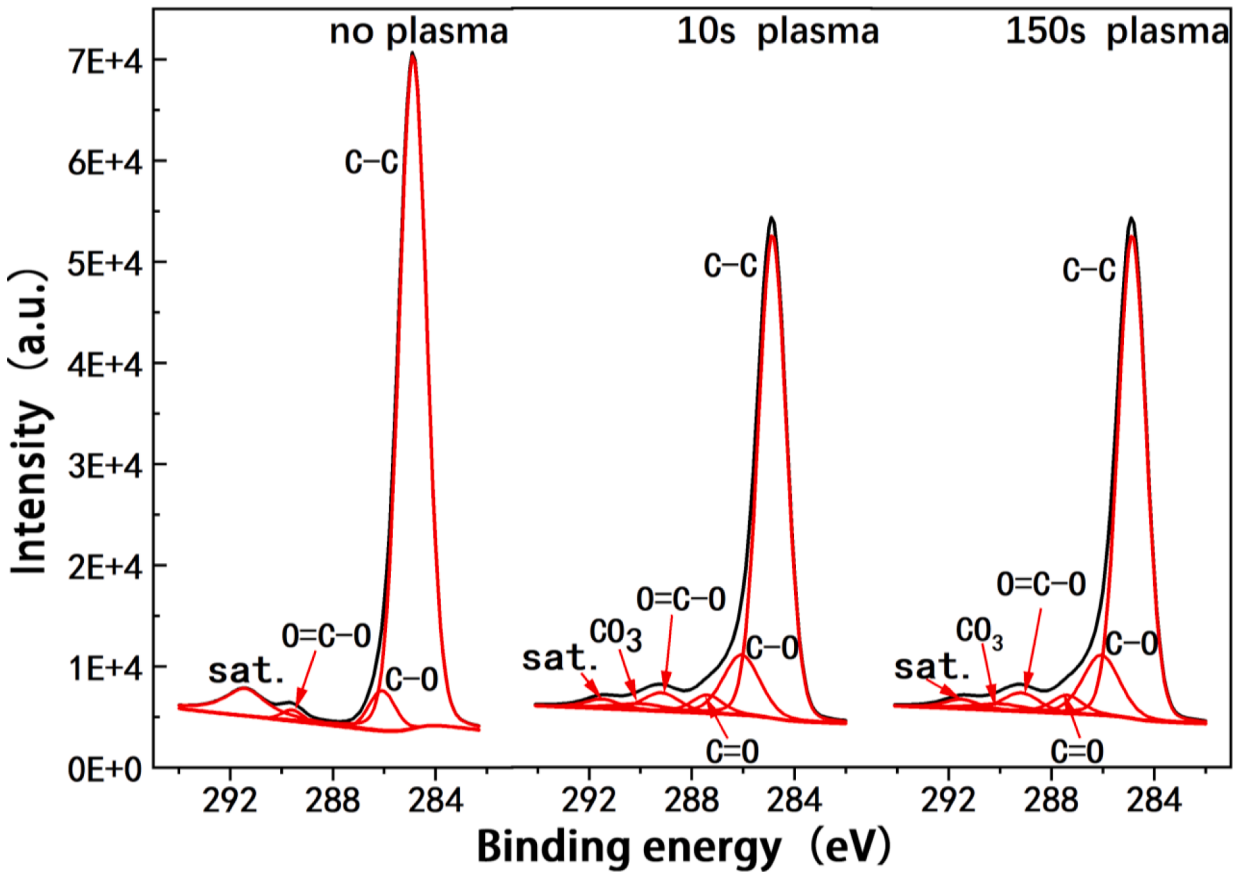

Fig. 4. XPS the fine structure of the C 1 s region for 0 s, 10 s, and 150 s oxygenated plasma treated PS particle monolayers on a thin gold film. The plasma power was 30 W, under 20 Pa pressure and 10 sccm O_2 and 20 sccm Ar gas flow.

and thus revealing a pristine silicon wafer surface (Fig. 2**A2**).

Similarly, plasma treatment at 10 W for 10 s also allowed for straightforward cleaning of the surface (**Figure S1B2**), because the plasma power and exposure time are not sufficient to shrink or alter the PS particle surface meaningfully. However, with incrementally increased plasma treatment power and duration (e.g., 10 W-150 s, 30 W-10 s, 30 W-150 s, 50 W-10 s, 50 W-150 s), the oxygen plasma treatment either induced or amplified surface crosslinking of the PS microsphere monolayer. As a result, the treated PS particles became resistant to THF, making dissolution challenging. Consequently, PS polymer residues persisted on the silicon wafer, yielding a milky white appearance (Fig. 2**B2,C2** and **Figure S1C2-E2**). It is important to underscore, however, that overly intense plasma treatment (e.g. 50 W-150 s) etched and shrinks the individual PS particles enough to create spacing between the PS particles (**Figure S2G**). This excess spacing hindered interconnectivity, resulting in facilitated particle detachment in the THF solvent as compared to less plasma treated PS particles, but more solvent resistance than in the case of pristine PS particles.

The observed solvent resistance was most pronounced in case of 30 W plasma power, which was chosen to further investigate the origins of this effect.

X-ray photoelectron spectroscopy (XPS) reveals the plasma-induced alteration in polymer chemistry [33]. The survey spectrum (Fig. 3) only shows evidence of the elements C and O from the PS polymer chain and Au from the substrate beneath the PS particles for both pristine and plasma-treated PS particle monolayers. The relative intensity of the O 1 s increases with plasma treatment duration and is indicative of the addition of oxygen-containing functional groups onto the polymer chain.

The high-resolution XPS spectrum of the C 1 s region (Fig. 4) shows that all samples are dominated by C—C (284.8 eV) contribution of the polymer backbone and with some contribution from O = C—O groups (288.8 eV). The presence of C—O and O = C—O groups in the pristine PS particle spectrum, despite the PS chemical formula being $(C_8H_8)_n$ and not containing oxygen atoms, are caused by oxygenated end-groups from PS particle synthesis, and by adventitious carbon contamination, which was minimized through short radiation exposure. It is important to note that the formation of hydroxyl and carboxyl groups in PS particle systems is not an aberration, but rather an inherent part of the synthesis process of colloidal PS particles. The polymerization pathway invariably leads to the creation of these oxygenated end-groups, which are instrumental in lending stability to the colloidal suspension. These groups facilitate the establishment of interparticle repulsive forces, which are pivotal for maintaining particle dispersion and preventing aggregation, thus playing a pivotal role in the stability of the PS colloidal system. The plasma treatment induces the formation of C = O groups (287.6 eV) and O-(C = O)-O groups (290.0 eV) and increased the relative intensity of the C—O group signal (281.1 eV). Simultaneously, the relative intensity of the π-π* oscillation peak (291.4 eV) contribution, which is associated with the benzene ring, is decreased and indicates polymer damage is not only restricted to the polymer backbone but also involves the breakage of the benzene ring, which can accommodate oxygenated groups [34,35].

The plasma-treatment-induced changes in the polymer chemistry are also evident from XPS valence spectra, which can be used for fingerprinting unique molecular species due to their unique spectral features [36].

The valance band spectra probe the density of states (DOS) at the sample surface and show characteristic peaks for specific energy regions (Fig. 5), which were normalized to the background at 33.9 eV [37]. The range between 0 and 10 eV corresponds to the C 2p orbital region of PS. However, in our case this region is dominated by the valence band signal of the Au 5d region because our PS particle monolayer sits on an Au film

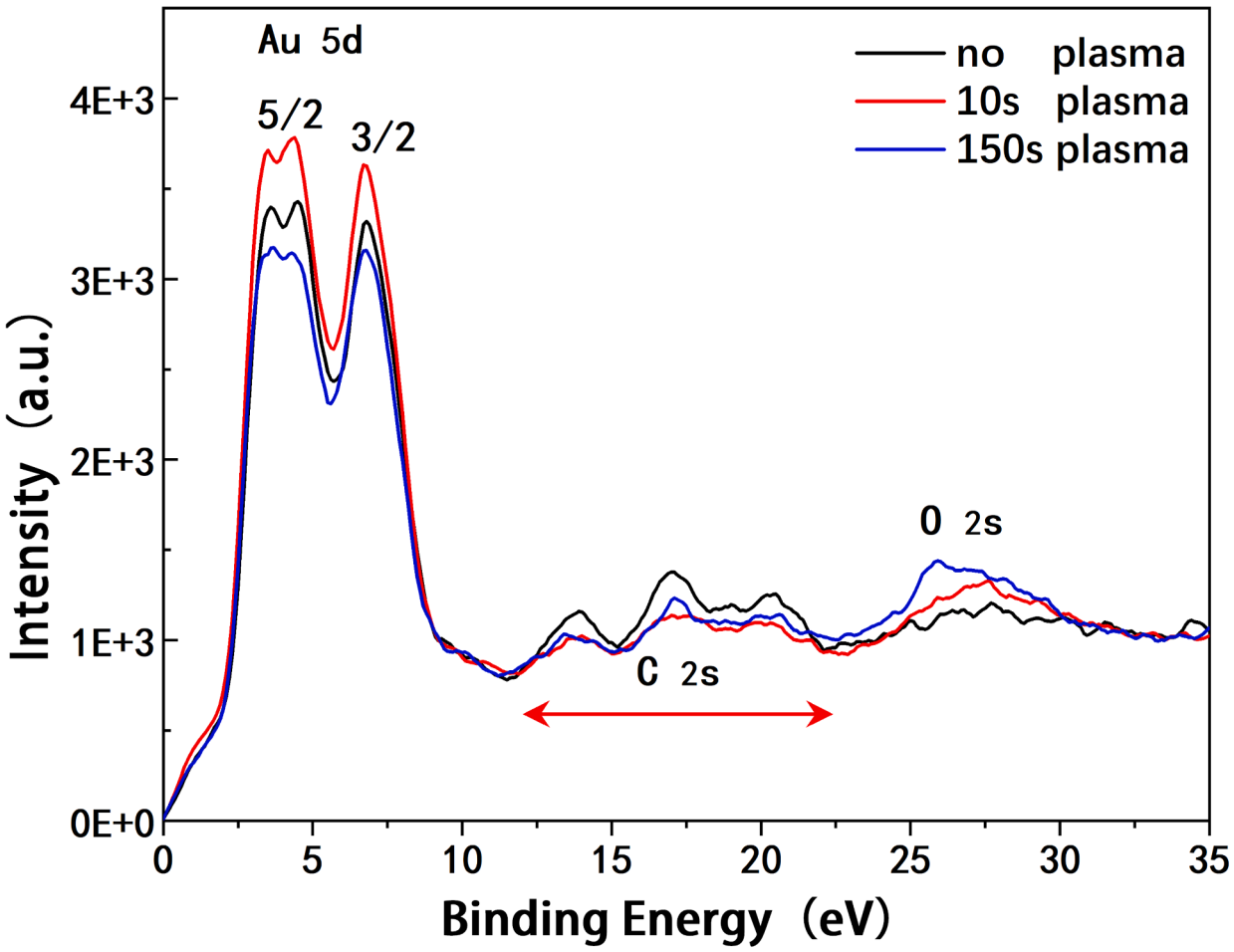

Fig. 5. XPS valence band spectra for 0 s, 10 s, and 150 s oxygenated plasma treated PS particle monolayers on a thin gold film. The plasma power was 30 W, under 20 Pa pressure and 10 sccm O_2 and 20 sccm Ar gas flow.

[38]. Au has a higher DOS than PS, which explains its domination despite the small, exposed Au surface between the PS particles [39]. The spectral characteristic peaks generated by the C 2 s orbital in the benzene ring can be seen in the range 13–20 eV and the prolonged plasma exposure results in the weakening of these features and can be interpreted in the opening of the benzene ring and the addition of oxygen-containing functional groups. At the same time, increased plasma exposure results in the increase of the O 2 s orbital region between 25 and 27 eV, which also clearly indicates the addition of oxygen-containing functional groups to the polymer surface [40,41].

Collectively, the XPS studies reveal a significant alteration in the chemistry of the PS polymer particles, characterized by the breakdown of the polymer backbone and benzene ring, and the introduction of oxygen-containing functional groups. Moreover, the occurrence of induced solvent resistance serves as indirect evidence of crosslinking between the polymer chains. All these changes in the polymer chemistry are attributable to the chemical and physical etching mechanisms resulting from the exposure of the PS particles to oxygenated plasma [42,43].

Oxygen plasmas are particularly effective in generating free oxygen radicals, which can adhere to the polymer chains and also lead to the severance of molecular bonds within the polymer chains. Physical ion collision with the polymer chain offers another potential cause for C—C and C—H bond breakage, culminating in the formation of dangling bonds capable of participating in crosslinking reactions.

Proceeding from the plasma-induced crosslinking on the PS particles surface, we utilized the ultra-thin cross-linked PS polymer layer to eliminate the bulk PS body and construct substrate-based microcavities. We electrodeposited copper through the unaltered and plasma-treated PS particle monolayers, [31] achieving a Cu thickness commensurate with half the PS particle diameter. With plasma-treated PS particles, the surface cross-linked films adhered to the copper formed around the PS particles or interconnected with one another, facilitated by the THF solvent, thus preventing their detachment. A detailed SEM image of each production step is shown in **Figure S3**.

The untreated PS particle monolayer swiftly dissolved in THF, leaving a periodic array of copper hemispheres behind (Fig. 6**A**). Similarly, after a brief, low-intensity plasma treatment at 10 W-10 s, the PS microsphere surfaces did not undergo sufficient cross-linking and were easily dissolved, resulting in a similar array of copper hemispheres **(Figure S2B)**.

However, increasing the plasma treatment duration to 150 s led to plasma-induced surface cross-linking of the PS particles. This rendered the microsphere surfaces solvent-resistant, preventing their dissolution in THF and enabling their retention on the hemisphere surface. It's noteworthy that due to the relatively low plasma intensity, the PS particles couldn't fully anchor to the surrounding metal bowls **(Figure S2C)**.

When the etching power was amplified to 30 W, the plasma-treated PS particle monolayer (Fig. 6**B**) left behind an ultra-thin cross-linked PS film over the copper hemisphere array (Fig. 6**C**) after prolonged solvent exposure. The integrity of this polymer films depends on the plasma exposure time. For 30 W-10 s plasma exposure the creation of a porous, cross-linked PS film of 48±6 nm thickness on the copper hemispheres was observed (**Figure S2D** and Fig. 7**A**). Analogously, a plasma treatment at 30 W-150 s led to the formation of a microcavity between the

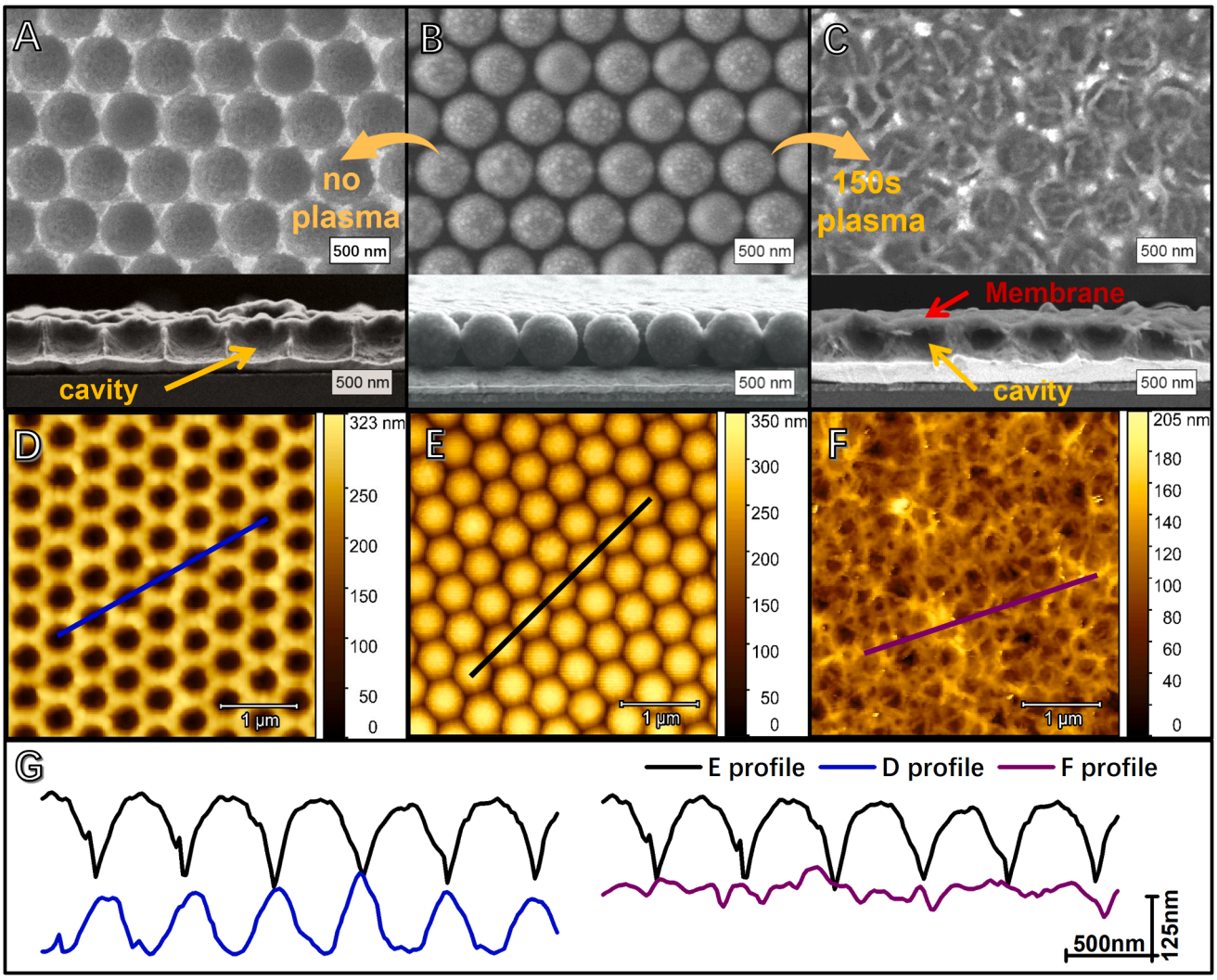

Fig. 6. A distinct change in the chemical composition of the PS is induced by the plasma. (A, B, C) SEM images showing the top-view and cross-section of (A) hemispherical metal cup array fabricated using an untreated (B) 500 nm diameter PS particle monolayer, and (C) a hemispherical metal cup array covered with an ultra-thin crosslinked polymer film fabricated using 150 s oxygenated plasma-treated PS particles. The polymer film is anchored to the metal bowls and encloses a cavity between the metal bowls and itself. (D, E, F) show AFM images corresponding to (A, B, C), and their respective color-coded profiles are shown in (G). The PS particle monolayer and metal bowls show inverse hemispherical profiles, while the ultra-thin crosslinked polymer film lies flat on the topography. The plasma power was 30 W, under 20 Pa pressure and 10 sccm O_2 and 20 sccm Ar gas flow.

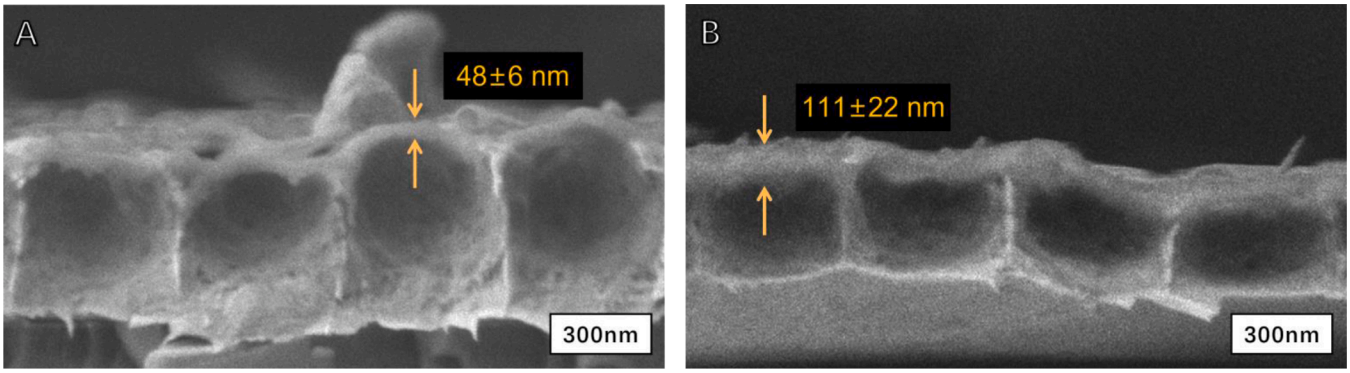

Fig. 7. Cross-section SEM images of substrate-based microcavity architecture produced from (A) 10 s and (B) 150 s oxygenated plasma-treated PS particle monolayers. Hemisphere copper bowls were electrodeposited and the bulk PS polymer of the PS particles was removed by soaking the material in THF for 24 h, which enabled the PS to diffuse through the cross-linked PS film spanning over the copper bowls The PS films are approximately 48 ± 6 nm and 111 ± 22 nm thick for 10 s and 150 s plasma-treatment time respectively. The plasma power was 30 W, under 20 Pa pressure and 10 sccm O_2 and 20 sccm Ar gas flow.

copper hemispheres and a closed, cross-linked polymer film of 111±22 nm thickness (**Figure S2E** and Fig. 7**B**).

However, it's crucial to highlight that excessive plasma treatment can induce adverse effects. This was observed at 50 W-10/150 s (**Figure S2F,G**), where the plasma treatment resulted in PS particle size reduction and a concurrent increase in spacing. This effectively broke the interconnectivity of the PS film resulting in their detachment in the solvent.

Overall, microcavities enclosed by intact PS polymer film were optimally obtained for plasma treatment with a power of 30 W for a duration of 150 s.

AFM measurements were conducted to demonstrate that these ultra-thin polymer films span over the hemispherical metal bowls and didn't sink into the cavities. Fig. 6**D** shows the surface topography of the periodic Cu hemisphere arrays, which were fabricated from an untreated PS particle monolayer (Fig. 6**E**) and correspond to the SEM image in Fig. 6**A** and Fig. 6**B**, respectively. As expected, these two structures show a periodic array of hemispheres, which are inverse in respect to each other. However, the surface topography of hemispherical metal bowls produced from 150 s plasma treated PS particle monolayers (Fig. 6**F**) is flat, demonstrating that the ultra-thin polymer film spans over the cavities that are enclosed between itself, and the hemisphere metal bowls. This indicates that the polymer films has good mechanical integrity and is permeable for organic solvents such as THF. The permeability for organic compounds is even large enough for not cross-linked polystyrene, i.e. very large molecules, to diffuse through the cross-linked polymer membrane, which is evidenced by the creation of the cavity below the polymer film. This offers remarkable opportunities to utilize these cavities as substrate based microreactors. Such microreactors could offer several advantages like: (i) photocatalyst particles could be enclosed in the cavities to build photocatalytic flow-cells; (ii) the hemisphere metal morphology could offer microlensing and light concentration effects; (iii) the ultra-thin polymer membranes could enable electrochemical reactions in a two-compartment cell with different immiscible solvents, which are separated by the polymer films. The key difficulty to achieve this is to load the active catalysts into the cavities. However, the preparation of composite PS microspheres has been reported, [44,45] which could be realized by doping the catalysts into the PS particles and releasing them in the final fabrication step when the PS particles are dissolved.

4. Conclusion

In conclusion, we have revealed that oxygenated plasma treatment of PS particles induces solvent resistance to organic solvents like THF, which dissolve untreated PS particles with ease. This solvent resistance is due to the modification of the polymer chemistry in an ultra-thin layer at the PS particle's surface, which is a result of cross-linking and oxygen-containing functional group addition after C–C bond cleavage and benzene ring opening as shown by XPS fine structure and valence band probing. Specifically, the C 1 s region showed a distinct change in the appearance of several oxygen-containing functional groups, such as hydroxyl, carboxyl, and carbonyl groups. The valence band spectra revealed a decrease of the C 2 s orbital contribution and an increase of the O 2 s orbital contribution at the same time. The resulting ultra-thin films can be tuned in thickness through the plasma exposure time, where its thickness varies from 48 ± 6 nm and 111 ± 22 nm for 10 s to 150 s plasma exposure respectively. The ultra-thin crosslinked PS films are permeable to THF and non-crosslinked PS chains and are therefore likely to be permeable for a large number of organic compounds. We exploited this feature to build substrate-based microcavity arrays that consists of a periodic array of electrodeposited metal hemispheres, which enclose the microcavities with the anchored membrane spanning over the cavity with good mechanical integrity. The proposed microreactor design offers opportunities for novel microreactor applications like photocatalytic flow-cell reactors utilizing the metal bowls as microlensing and light concentrator arrays. The placement of catalyst particles into the microcavities could be achieved by doping PS microspheres with inorganic catalyst particles, which remain in the cavity during PS particles dissolution and will be explored in the future.

Author contributions

The manuscript was written through contributions of all authors. All authors have given approval to the final version of the manuscript.

Supporting information

Figure S1 shows a self-assembled PS microsphere array on a silicon wafer is shown before and after being etched by untreated and different intensity oxygen plasma, and then briefly dissolved by THF. Figure S2 shows SEM images depicting of The PS microsphere array was subjected to oxygenated plasma etching at different power and time settings, followed by electro-deposition of copper and dissolution of PS microspheres in THF for 24 h. Figure S3 shows a gallery of SEM images corresponding to all the involved processing steps.

CRediT authorship contribution statement

Caitao Li: Investigation, Formal analysis, Visualization, Writing – original draft. **Tengfei Qiu:** Supervision, Investigation, Writing – review & editing. **Guofu Zhou:** Resources, Data curation, Writing – review & editing, Funding acquisition. **Michael Giersig:** Supervision, Validation, Writing – review & editing, Funding acquisition. **Xin Wang:** Methodology, Writing – review & editing, Funding acquisition. **Eser Metin Akinoglu:** Supervision, Writing – original draft, Conceptualization, Methodology.

Declaration of Competing Interest

The authors declare that they have no known competing financial interests or personal relationships that could have appeared to influence the work reported in this paper.

Data availability

All data is included in the manuscript.

Acknowledgement

This work has been funded by the Guangdong Innovative and Entrepreneurial Team Program (No. 2016ZT06C517), the Science and Technology Program of Guangdong (No.2021A0505030014), the Science and Technology Program of Guangzhou (No. 2019050001), the Program for Chang Jiang Scholars and Innovative Research Teams in Universities (No. IRT_17R40), the Guangdong Provincial Key Laboratory of Optical Information Materials and Technology (No. 2017B030301007), the National Center for International Research on Green Optoelectronics (Nos. 2016B01018, 2022A0505090010) , the MOE International Laboratory for Optical Information Technologies and the 111 Project. T.Q. thanks the support from the UQ Development Fellowship (UQFEL1832321).

Supplementary materials

Supplementary material associated with this article can be found, in the online version, at doi:10.1016/j.surfin.2023.103164.

References

[1] W. Wang, L. Qi, Light Management with Patterned Micro- and Nanostructure Arrays for Photocatalysis, Photovoltaics, and Optoelectronic and Optical Devices, Adv. Funct. Mater. 29 (2019), 1807275.

[2] M. Zahedinejad, A.A. Awad, S. Muralidhar, R. Khymyn, H. Fulara, H. Mazraati, M. Dvornik, J. Åkerman, Two-dimensional mutually synchronized spin Hall nano-oscillator arrays for neuromorphic computing, Nat. Nanotechnol. 15 (2020) 47–52.

[3] E. Metin Akinoglu, T. Sun, J. Gao, M. Giersig, Z. Ren, K. Kempa, Evidence for critical scaling of plasmonic modes at the percolation threshold in metallic nanostructures, Appl. Phys. Lett. 103 (2013), 171106.

[4] H. Lee, K. Song, M. Lee, J.Y. Park, Situ Visualization of Localized Surface Plasmon Resonance-Driven Hot Hole Flux, Adv. Sci. 7 (2020), 2001148.

[5] C.-L. Luo, R.-X. Yang, W.-G. Yan, C.-M. Chen, S.-Y. Liu, S.-J. Zhao, W.-Q. Ge, Z.-F. Liu, G.-Z. Jia, Surface Plasmon-Enhanced Luminescence of CdSe/CdS Quantum Dots Film Based on Au Nanoshell Arrays, Materials (Basel) 12 (2019) 362.

[6] H.M. Luong, M.T. Pham, B. Ai, T.D. Nguyen, Y. Zhao, Magnetoplasmonic properties of Ag-Co composite nanohole arrays, Phys. Rev. B. 99 (2019), 224413.

[7] T. Qiu, E.M. Akinoglu, B. Luo, M. Konarova, J. Yun, I.R. Gentle, L. Wang, Nanosphere Lithography: a Versatile Approach to Develop Transparent Conductive Films for Optoelectronic Applications, Adv. Mater. 34 (2022), 2103842.

[8] T. Qiu, B. Luo, E.M. Akinoglu, J. Yun, I.R. Gentle, L. Wang, Trilayer Nanomesh Films with Tunable Wettability as Highly Transparent, Flexible, and Recyclable Electrodes, Adv. Funct. Mater. 30 (2020), 2002556.

[9] M. Gao, M. Cho, H.-J. Han, Y.S. Jung, I. Park, Palladium-Decorated Silicon Nanomesh Fabricated by Nanosphere Lithography for High Performance, Room Temperature Hydrogen Sensing, Small 14 (2018), 1703691.

[10] Y.-F.C. Chau, K.-H. Chen, H.-P. Chiang, C.M. Lim, H.J. Huang, C.-H. Lai, N.T.R. N. Kumara, Fabrication and Characterization of a Metallic–Dielectric Nanorod Array by Nanosphere Lithography for Plasmonic Sensing Application, Nanomaterials 9 (2019) 1691.

[11] W. Wang, J. Dong, X. Ye, Y. Li, Y. Ma, L. Qi, Heterostructured TiO_2 Nanorod@Nanobowl Arrays for Efficient Photoelectrochemical Water Splitting, Small 12 (2016) 1469–1478.

[12] R. Brisbin, J. Zhou, T. Bond, L. Voss, A.J. Simon, R. Baxter, A.S.P. Chang, Plasmonics-Enhanced UV Photocatalytic Water Purification, J. Phys. Chem. C. 125 (2021) 9730–9735.

[13] C. Salinas, E. Rodríguez-Sevilla, E. Flores-Romero, J.-C. Cheang-Wong, Fabrication and Characterization of Surfaceenhanced Raman Scattering Substrates With Ordered Arrays of Gold Nanopyramids By Means of Nanosphere Lithography, Mater. Express. 9 (2019) 141–149.

[14] C.-C. Ho, K. Zhao, T.-Y. Lee, Quasi-3D gold nanoring cavity arrays with high-density hot-spots for SERS applications via nanosphere lithography, Nanoscale 6 (2014) 8606–8611.

[15] P.-H. Lei, P.-C. Yang, P.-C. Huang, Investigation of Photonic-Crystal-Structured p-GaN Nanorods Fabricated by Polystyrene Nanosphere Lithography Method to Improve the Light Extraction Efficiency of InGaN/GaN Green Light-Emitting Diodes, Materials (Basel) 14 (2021) 2200.

[16] X. Fang, C. Zheng, Z. Yin, Z. Wang, J. Wang, J. Liu, D. Luo, Y.J. Liu, Hierarchically Ordered Silicon Metastructures from Improved Self-Assembly-Based Nanosphere Lithography, ACS Appl. Mater. Interfaces. 12 (2020) 12345–12352.

[17] M. Kaya, M.F. Dilekoğlu, Ö. Şahin, C. Saka, Plasma Treated Sepiolite: a New Adsorbent for Removal of Malachite Green from Contaminated Water, Plasma Chem, Plasma Process 36 (2016) 1417–1430.

[18] G.Elçi Ölçenoğlu, C. Saka, Surface modification of coal sample with oxygen plasma treatment, Surf. Eng. 36 (2020) 531–538.

[19] Ö. Şahin, Y. Yardim, O. Baytar, C. Saka, Enhanced electrochemical double-layer capacitive performance with CO_2 plasma treatment on activated carbon prepared from pyrolysis of pistachio shells, Int. J. Hydrog. Energy. 45 (2020) 8843–8852.

[20] C. Saka, O. Baytar, Y. Yardim, Ö. Şahin, Improvement of electrochemical double-layer capacitance by fast and clean oxygen plasma treatment on activated carbon as the electrode material from walnut shells, Biomass Bioenergy 143 (2020), 105848.

[21] E.M. Akinoglu, A.J. Morfa, M. Giersig, Understanding Anisotropic Plasma Etching of Two-Dimensional Polystyrene Opals for Advanced Materials Fabrication, Langmuir 30 (2014) 12354–12361.

[22] M. Domonkos, P. Demo, A. Kromka, Nanosphere Lithography for Structuring Polycrystalline Diamond Films, Crystals 10 (2020) 118.

[23] D. Darvill, M. Iarossi, R.M. Abraham Ekeroth, A. Hubarevich, J.-A. Huang, F. De Angelis, Breaking the symmetry of nanosphere lithography with anisotropic plasma etching induced by temperature gradients, Nanoscale Adv. 3 (2021) 359–369.

[24] K. Wang, C. Li, Z. Li, H. Li, A. Li, K. Li, X. Lai, Q. Liao, F. Xie, M. Li, Y. Song, A facile fabrication strategy for anisotropic photonic crystals using deformable spherical nanoparticles, Nanoscale 11 (2019) 14147–14154.

[25] L.P. Rao Pala, N.R. Peela, Green Hydrogen Production in an Optofluidic Planar Microreactor via Photocatalytic Water Splitting under Visible/Simulated Sunlight Irradiation, Energy Fuels 35 (2021) 19737–19747.

[26] E.V. Ovchinnikova, N.V. Vernikovskaya, A.G. Gribovskii, V.A. Chumachenko, Multichannel microreactors for highly exothermic catalytic process: the influence of thermal conductivity of reactor material and of transport phenomena inside the channels on the process efficiency, Chem. Eng. J. 409 (2021), 128046.

[27] X. Yao, Y. Zhang, L. Du, J. Liu, J. Yao, Review of the applications of microreactors, Renew. Sustain. Energy Rev. 47 (2015) 519–539.

[28] M.I. Domínguez, M.A. Centeno, M. Martínez T, L.F. Bobadilla, Ó.H. Laguna, J. A. Odriozola, Current scenario and prospects in manufacture strategies for glass, quartz, polymers and metallic microreactors: a comprehensive review, Chem. Eng. Res. Des. 171 (2021) 13–35.

[29] P. Rambabu, S. Patel, D. Gogoi, R.V.S. Uppaluri, N.R. Peela, Optofluidic microreactor for the photocatalytic water splitting to produce green hydrogen, Int. J. Hydrog. Energy. 47 (2022) 2152–2163.

[30] E.J.S. Brás, V. Chu, J.P. Conde, P. Fernandes, Recent developments in microreactor technology for biocatalysis applications, React. Chem. Eng. 6 (2021) 815–827.

[31] X. Meng, Y. Song, T. Shu, Morphology control and optical characterization of three-dimensional ordered macroporous Cu films from template-assisted electrodeposition, J. Porous Mater. 27 (2020) 1069–1076.

[32] D. Grujicic, B. Pesic, Electrodeposition of copper: the nucleation mechanisms, Electrochim. Acta 47 (2002) 2901–2912.

[33] L.J. Gerenser, XPS studies of in situ plasma-modified polymer surfaces, J. Adhes. Sci. Technol. 7 (1993) 1019–1040.

[34] Y. Fukunaga, R.C. Longo, P.L.G. Ventzek, B. Lane, A. Ranjan, G.S. Hwang, G. Hartmann, T. Tsutsumi, K. Ishikawa, H. Kondo, M. Sekine, M. Hori, Interaction of oxygen with polystyrene and polyethylene polymer films: a mechanistic study, J. Appl. Phys. 127 (2020), 023303.

[35] R.C. Longo, A. Ranjan, P.L.G. Ventzek, Density Functional Theory Study of Oxygen Adsorption on Polymer Surfaces for Atomic-Layer Etching: implications for Semiconductor Device Fabrication, ACS Appl. Nano Mater. 3 (2020) 5189–5202.

[36] W.R. Salaneck, Photoelectron spectroscopy of the valence electronic structure of polymers, Crit. Rev. Solid State Mater. Sci. 12 (1984) 267–296.

[37] R.M. France, R.D. Short, Plasma Treatment of Polymers: the Effects of Energy Transfer from an Argon Plasma on the Surface Chemistry of Polystyrene, and Polypropylene. A High-Energy Resolution X-ray Photoelectron Spectroscopy Study, Langmuir 14 (1998) 4827–4835.

[38] J.D. Andrade, X-ray photoelectron spectroscopy (XPS), Surf. Interfacial Asp. Biomed. Polym. 1 (1985) 105–195. Surf. Chem. Phys.

[39] V.J. Keast, R.L. Barnett, M.B. Cortie, First principles calculations of the optical and plasmonic response of Au alloys and intermetallic compounds, J. Phys. Condens. Matter. 26 (2014), 305501.

[40] J. Riga, J.-J. Pireaux, J.J. Verbist, An ESCA study of the electronic structure of solid benzene.: valence levels, core level and shake-up satellites, Mol. Phys. 34 (1977) 131–143.

[41] R. Foerch, G. Beamson, D. Briggs, XPS valence band analysis of plasma-treated polymers, Surf. Interface Anal. 17 (1991) 842–846.

[42] E.M. Liston, L. Martinu, M.R. Wertheimer, Plasma surface modification of polymers for improved adhesion: a critical review, J. Adhes. Sci. Technol. 7 (1993) 1091–1127.

[43] H. Schonhorn, F.W. Ryan, R.H. Hansen, Surface treatment of polypropylene for adhesive bonding, J. Adhes. 2 (1970) 93–99.

[44] R.Y. Hong, B. Feng, G. Liu, S. Wang, H.Z. Li, J.M. Ding, Y. Zheng, D.G. Wei, Preparation and characterization of Fe_3O_4/polystyrene composite particles via inverse emulsion polymerization, J. Alloys Compd. 476 (2009) 612–618.

[45] R.L. Sherman, W.T. Ford, Semiconductor Nanoparticle/Polystyrene Latex Composite Materials, Langmuir 21 (2005) 5218–5222.